INSTITUTE OF PHYSICS PUBLISHING SMART MATERIALS AND STRUCTURES
Smart Mater. Struct. **15** (2006) 1085–1093 doi:10.1088/0964-1726/15/4/022

Modeling and testing of PZT and PVDF piezoelectric wafer active sensors

B Lin and V Giurgiutiu

University of South Carolina, 300 Main Street, Columbia, SC 29208, USA

E-mail: linbin@engr.sc.edu and victorg@sc.edu

Received 12 August 2005, in final form 24 April 2006
Published 7 July 2006
Online at stacks.iop.org/SMS/15/1085

Abstract
Piezoelectric wafer active sensors (PWAS) used in structural health monitoring (SHM) applications are able to detect structural damage using Lamb waves. PWAS are small, lightweight, unobtrusive and inexpensive. They achieve direct transduction between electric and elastic wave energies. PWAS are charge mode sensors and can be used as both transmitters and receivers. The focus of this paper is to find a suitable *in situ* piezoelectric active sensor for sending and receiving Lamb waves to be used in the SHM of structures with a curved surface. Current SHM technology uses brittle piezoceramic (PZT) wafer active sensors. Since piezoceramics are brittle, this approach could only be used on flat surfaces. The motivation of our research was to explore the use of flexible piezoelectric materials, e.g. piezoelastic polymers such as PVDF. However, PVDF stiffness is orders of magnitude lower than the PZT stiffness, and hence PVDF Lamb wave transmitters are much weaker than PZT transmitters. Thus, our research proceeded in two main directions: (a) to model and understand how piezoelectric material properties affect the behaviour of piezoelectric wafer active sensors; and (b) to perform experiments to test the capabilities of the flexible PVDF PWAS in comparison with those of stiffer but brittle PZT PWAS. We have shown that, with appropriate signal amplification, PVDF PWAS can perform the same Lamb wave transmission and reception functions currently performed by PZT PWAS. The experimental results of PZT-PWAS and PVDF-PWAS have been compared with a conventional strain gauge. The theoretical and experimental results in this study gave a basic demonstration of the piezoelectricity of PZT-PWAS and PVDF-PWAS.

(Some figures in this article are in colour only in the electronic version)

1. Introduction

Structural health monitoring (SHM) addresses an urgent need of our aging infrastructure. SHM sets out to determine the health of a structure by reading a network of sensors that are embedded into the structure and monitored over time. SHM can be either passive or active. Passive SHM infers the state of the structure using passive sensors that are monitored over time and fed into a structural model. Examples of passive SHM are the monitoring of loads, stress, environmental conditions, and acoustic emission from cracks utilizing an assortment of sensors such as acoustic emission transducers, resistance strain gauges, fibre-optic strain gauges, filament crack gauges, and corrosive environment sensors. Active SHM uses active sensors that interrogate the structure to detect the presence of damage, and to estimate its extent and intensity.

1.1. The use of PWAS in structural health monitoring

One active SHM method employs piezoelectric wafer active sensors, which send and receive ultrasonic Lamb waves and determine the presence of cracks, delaminations, disbands, and corrosion. In recent years investigators (Chang [1, 2], Wang and Chang [3], Lin and Yuan [4, 5], Ihn and Chang [6], Giurgiutiu *et al* [7–9], and others) have explored the generation and detection of structural waves with PWAS. Most of

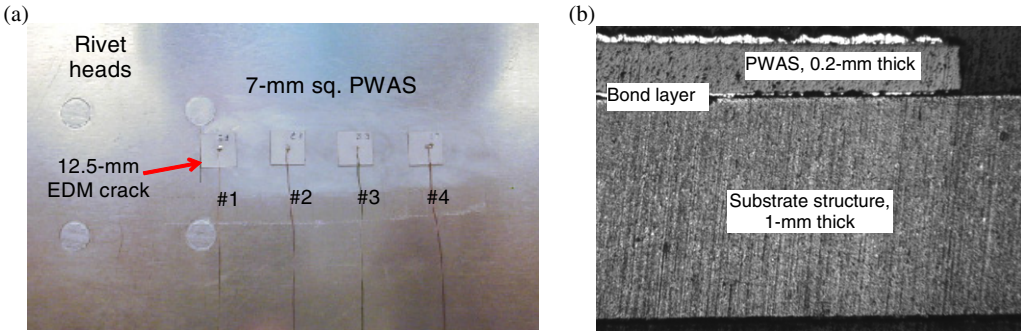

Figure 1. (a) PWAS mounted on an aircraft panel; (b) PWAS were attached to a substrate structure through the adhesive bond layer, which was susceptible to environmental attacks.

the methods used in conventional non-destructive evaluation (NDE), such as pitch-catch, pulse-echo, and phased arrays, have also been demonstrated experimentally with PWAS [8, 9]. These successful experiments have positioned PWAS as an enabling technology for the development and implementation of active SHM systems. PWAS are inexpensive, non-intrusive, unobtrusive, and minimally invasive. They can be surface-mounted on existing structures, inserted between the layers of lap joints, or placed inside composite materials.

Figure 1 shows an array of 7 mm square PWAS mounted on an aircraft panel, adjacent to rivet heads and an electric discharge machined (EDM) simulated crack. The minimally invasive nature of the PWAS devices is apparent. A PWAS is much lighter, smaller and cheaper in contrast to a conventional ultrasonic transducer. PWAS are used in SHM applications and are able to detect structural damage using Lamb waves. They achieve direct transduction between electric and elastic wave energies. PWAS are essential elements in Lamb-wave SHM with pitch-catch, pulse-echo, phased array and electromechanical (E/M) impedance methods.

1.2. Practical issues in PWAS design and construction

PWAS can be made from piezoceramics, piezocomposites, or piezopolymers. The most common PWAS are made of piezoceramics (e.g. lead zirconate titanate, also known as PZT). Piezoceramics are typically made of simple perovskites and solid-solution perovskite alloys. Mechanical compression or tension on a poled piezoelectric ceramic element changes the dipole moment, creating a voltage. Compression along the direction of polarization or tension perpendicular to the direction of polarization generates a voltage of the same polarity as the poling voltage.

Brittle PZT-PWAS can withstand very little bending. This brittleness imposes difficulties in handling and bonding of the PWAS onto the structure being monitored. In addition, they have poor conformability to curved surfaces, and local straightening of the structural surface is required for PWAS installation [10–12].

Composite PWAS are made by dispersing electroactive, magnetoactive [13, 14, 23], or piezoelectric [12, 15, 16] particles (powders) in polymeric matrix materials. The resulting particulate composite displays effective piezoelectric or piezomagnetic properties that are somehow dependent on the volume ratio. However, the connectivity and the interfacial bond between the phases also play a considerable role. Recent research interest has been shown in the combination of electroactive and magnetoactive effects into a more complex composite that displays both electroactive and magnetoactive responses [17–21]. These composites, which have a three-way coupling between the electric, magnetic, and elastic fields, are known as magnetoelectric or multiferroic composites.

Piezopolymers (e.g. polyvinylidene fluoride, also known as PVDF) are a class of piezoelectric materials that display piezoelectric properties similar to those of quartz and piezoceramics [22]. PVDF are supplied in the form of thin films that are flexible and show large compliance. They are less expensive and easier to fabricate than piezoceramics. The flexibility of PVDF-PWAS overcomes some of the drawbacks associated with the brittleness of the piezoelectric ceramics.

When PWAS are used as active sensors to generate and receive the Lamb wave, the received signal is small and has a lot of noise, especially when the test structure is thick. Traditionally, wideband amplifiers are used to provide a high input voltage to generate stronger Lamb waves, but the input voltage cannot go beyond the PWAS voltage limitation. A more efficient way is to amplify the PWAS output signals. The principle of a charge amplifier for PWAS applications is introduced in detail below, and the experimental results agree very well with the theoretical model of this charge amplifier.

In this paper, we will analyse the PWAS model and experimentally verify the model with vibration and impact detection using PZT-PWAS and PVDF-PWAS. A PWAS charge amplifier is also modelled and tested in the application of PZT-PWAS and PVDF-PWAS. The focus of this paper is to find a suitable *in situ* piezoelectric active sensor for sending and receiving Lamb waves to be used in the SHM of structures with curved surfaces. The motivation of our research was to explore the use of piezoelastic polymer PVDF. However, PVDF stiffness is orders of magnitude lower than the PZT stiffness, and hence PVDF Lamb wave transmitters are much weaker than PZT transmitters. Thus, our research proceeded in two main directions: (a) to model and understand how piezoelectric material properties affect the behaviour of PWAS; and (b) to perform experiments to test the capabilities of the flexible PVDF PWAS in comparison with those of stiffer but brittle PZT PWAS. We have shown that, with appropriate signal amplification, PVDF PWAS can perform the same Lamb wave transmission and reception functions currently performed by PZT PWAS.

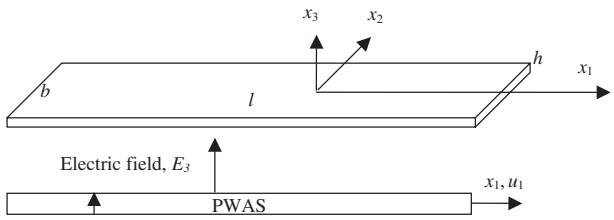

Figure 2. Schematic of a piezoelectric wafer active sensor.

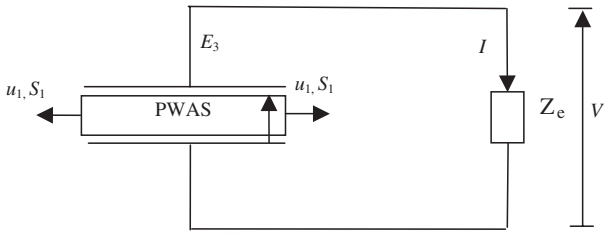

Figure 3. Schematic of a PWAS connected with measurement equipment (resistance Ze).

2. Modeling

2.1. Linear piezoelectricity equation

In conventional ultrasonics, guided waves are generated by impinging the structural surface obliquely with an ultrasonic beam from a relatively large ultrasonic transducer affixed to a wedge. Snell's law ensures mode conversion at the interface, hence a combination of pressure and shear waves are simultaneously generated in the structure. If the structure is thin-walled, then guided plate or shell waves are created. Alternatively, guided waves can be generated with a comb transducer, having comb spacing tuned with the guided-wave half wavelength. However, these conventional Lamb-wave probes (wedge and comb transducers) are relatively heavy, bulky, and expensive. In recent years, piezoelectric wafers permanently attached to the structure have been used for the guided waves' generation and detection. PWAS operated on the piezoelectric principle that couples the electrical and mechanical variables in the material, mechanical strain, (S_{ij}), mechanical stress, (T_{ij}), electrical field, (E_k), and electrical displacement (D_j), in the form:

$$S_{ij} = s^E_{ijkl} \cdot T_{kl} + d_{kij} \cdot E_k \tag{1}$$

$$D_j = d_{jkl} \cdot T_{kl} + \varepsilon^T_{jk} \cdot E_k \tag{2}$$

where s^E_{ijkl} is the mechanical compliance of the material measured at zero electric field, ε^T_{jk} refers to the dielectric permittivity measured at zero mechanical stress, and d_{kij} represents the piezoelectric coupling effect. For embedded NDE applications, PWAS couple their in-plane motion, excited by the applied oscillatory voltage through the piezoelectric effect, with the Lamb waves' particle motion on the material surface. Lamb waves can be either quasi-axial (S_0, S_1, S_2 ...), or quasi-flexural (A_0, A_1, A_2 ...).

2.2. PWAS actuator

Consider a piezoelectric wafer of length l, width b, and thickness h that is undergoing longitudinal expansion (u_1) induced by the thickness polarization electric field (E_3), (figure 2). The electric field is produced by the application of a harmonic voltage, $V(t) = \hat{V}e^{i\omega t}$, between the top and bottom surfaces (electrodes). Assume that the length, width and thickness have widely separated values ($h \ll b \ll l$) such that the length, width and thickness motions are practically uncoupled. Under the one-dimensional assumptions, the general constitutive equations reduce to the simpler expressions

$$S_1 = s_{11} \cdot T_1 + d_{31} \cdot E_3 \tag{3}$$

$$D_3 = d_{31} \cdot T_1 + \varepsilon_{33} \cdot E_3. \tag{4}$$

At zero mechanical stress T_1, the actuated strain is,

$$S_1 = d_{31} \cdot \frac{V(t)}{h}. \tag{5}$$

2.3. PWAS sensor

PWAS in the dynamic regime was also analysed by using one-dimensional assumptions. If one PWAS is undergoing longitudinal expansion (u_1) (figure 3), the resulting voltage is harmonic with frequency ω when vibration is harmonic with natural frequency ω.

For compactness, the notation used is:

$$\frac{\partial}{\partial t}() = \dot{()}. \tag{6}$$

For harmonic voltage, $\dot{V} = i\omega V$.

Consider the harmonic dynamic regime under the one-dimensional assumptions; the general constitutive equations are reduced to the simpler expressions:

$$\dot{S}_1 = s_{11} \cdot \dot{T}_1 + d_{31} \cdot \dot{E}_3 \tag{7}$$

$$\dot{D}_3 = d_{31} \cdot \dot{T}_1 + \varepsilon_{33} \cdot \dot{E}_3. \tag{8}$$

When PWAS is under harmonic strain and connected with external measurement equipment, it will generate an ac current in the circuit. The ac current can be expressed by using:

$$I = \dot{D}_3 \cdot A \tag{9}$$

$$I = V \cdot Y_e \tag{10}$$

where Y_e is the external admittance, and A is the PWAS surface area, $A = l \cdot b$.

Using Kirchhoff's current law for a closed circuit, we obtain the relation between voltage and stress:

$$V = \frac{A \cdot d_{31}}{Y_e + Y_0} \dot{T}_1 \tag{11}$$

where Y_0 is PWAS admittance, $Y_0 = i\omega\varepsilon_{33}\frac{A}{h}$.

From equation (3), we obtain

$$\dot{T}_1 = \frac{1}{s_{11}}\left(\dot{S}_1 + \frac{d_{31}}{h}\dot{V}\right). \tag{12}$$

Finally, we obtain the resulting voltage from the strain:

$$V = \frac{1}{Y_e + (1 - k^2_{31})Y_0} \cdot A\frac{d_{31}}{s_{11}}\dot{S}_1 \tag{13}$$

where k_{31} is the electromechanical coupling coefficient.

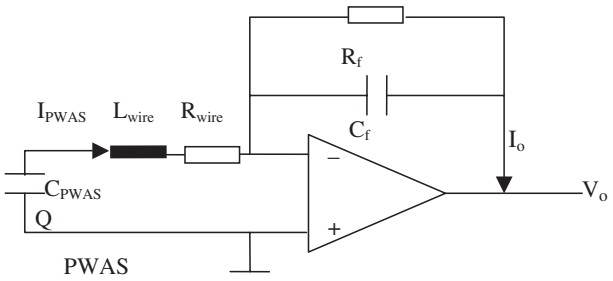

Figure 4. Schematic model of a charge amplifier consists of an op-amp amplifier and some passive components.

2.4. PWAS charge amplifier

In pitch-catch, pulse-echo and phased array applications, PWAS are used to generate and receive Lamb waves. The PWAS response is small, and we need to use the amplifier to get a good signal. The high-voltage amplifier can be used to provide a high excitation signal to the transmitter. The typical PWAS voltage limitation is in the range between −30 V and +120 V. An efficient way to amplify the signal is to use the charge amplifier after the receiver PWAS. The charge amplifier principle was patented by Kistler in 1950 and gained practical significance in the 1960s [29]. Basically, a charge amplifier consists of a high-gain inverting voltage amplifier at its input to achieve high insulation resistance. PWAS measuring systems are active electrical systems. That is, PWAS produce electrical output signals only when they experience a change in load. PWAS can be considered as a charge mode device with a capacitor C_{PWAS}.

The PWAS charge amplifier is shown in figure 4, including the wire resistance and inductance. The charge amplifier voltage output for a static load is

$$V_{\mathrm{o}} = -\frac{Q_{\mathrm{PWAS}}}{C_f}. \tag{14}$$

For a dynamic load,

$$I_{\mathrm{PWAS}} = V_{\mathrm{PWAS}} \frac{Y_{\mathrm{PWAS}} \cdot Y_{\mathrm{wire}}}{Y_{\mathrm{PWAS}} + Y_{\mathrm{wire}}} \tag{15}$$

$$I_{\mathrm{o}} = -V_{\mathrm{o}} Y_f \tag{16}$$

where

$$Y_{\mathrm{PWAS}} = \mathrm{j}\omega C_{\mathrm{PWAS}} \tag{17}$$

$$Y_f = \mathrm{j}\omega C_f + \frac{1}{R_f} \tag{18}$$

$$Y_{\mathrm{wire}} = \frac{1}{R_{\mathrm{wire}} + \mathrm{j}\omega L_{\mathrm{wire}}}. \tag{19}$$

The relation between charge amplifier output voltage V_{o} and PWAS output voltage V_{PWAS} is

$$V_{\mathrm{o}} = -\frac{Y_{\mathrm{PWAS}} \cdot Y_{\mathrm{wire}}}{Y_f (Y_{\mathrm{PWAS}} + Y_{\mathrm{wire}})} V_{\mathrm{PWAS}}. \tag{20}$$

3. Experiments

3.1. Cantilever beam free vibration

3.1.1. Experimental setup. Cantilever beams were well studied by Voltera [25, 26]. A typical cantilever beam, used in this study, is $L = 300$ mm long, $w = 19.2$ mm wide, and $t = 3.23$ mm thick. When the force P is removed from a displaced beam, the beam will return to its original shape. However, the inertia of the beam will cause the beam to vibrate around that initial location. According to the vibration and boundary equation, we can calculate the resonant frequency. The beam material is stainless steel 304 with density 8030 kg m^{-3} and Young's modulus $E = 195$ Gpa. Theoretically, the first three nature frequencies are $f_1 = 28.6$ Hz, $f_2 = 179$ Hz, and $f_3 = 501.3$ Hz.

The PZT-PWAS, PVDF-PWAS and strain gauge for dynamic measurement were investigated based on a vibration test setup show in figure 5. The beam was mounted as a cantilever in a calibrated cantilever fixture. Two 7 mm square PVDF-PWAS with different thicknesses were placed on the top of the beam; a 7 mm square PZT-PWAS and a strain gauge were placed at the bottom of the beam (figure 5(b)).

The tip of the beam was displaced to a certain value (approximately 10 mm) and then suddenly released as the beam entered in free vibration. A four-channel Tektronix TDS5030B oscilloscope was used to collect the vibration response from different kinds of sensors. Channel one was connected to the Vishay P3 strain indicator to record the electric signal generated by the resistance change in the strain gauge due to strain elongation. The other three channels were connected directly to the PZT-PWAS and PVDF-PWAS to record the electric signals generated through the piezoelectric coupling between the mechanical vibration and the electric field. The recorded traces are shown in figure 6. The Fourier transform was used to analyse the frequency contents of the signals, which should correspond to the natural free vibration frequencies of the cantilever beam. The resulting spectra are shown in figure 7. The first three natural frequencies are shown to be $f_1 = 29.7$ Hz, $f_2 = 181$ Hz, and $f_3 = 501$ Hz. The

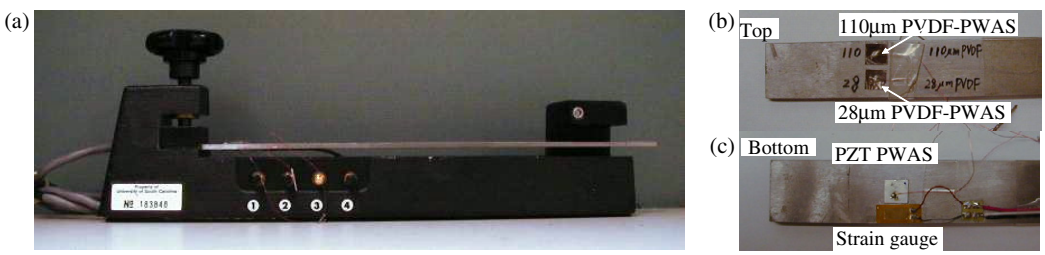

Figure 5. PZT-PWAS, PVDF-PWAS, and strain gauge on a cantilever beam: (a) experimental setup; (b) close-up view of the bottom surface showing the 200 μm PZT-PWAS and strain gauge; (c) close-up view of the top surface showing the 28 μm and 110 μm PVDF-PWAS.

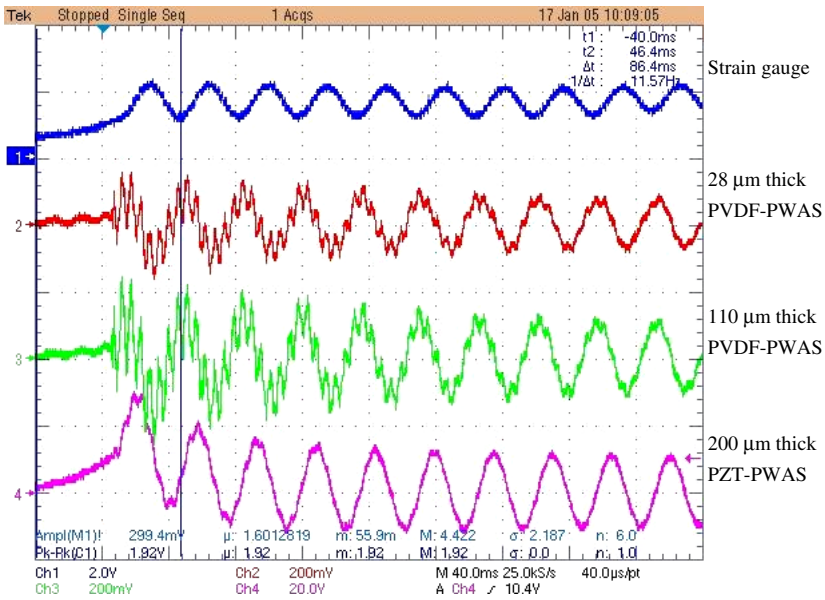

Figure 6. Vibration signal recorded by strain gauge, PVDF-PWAS and PZT-PWAS.

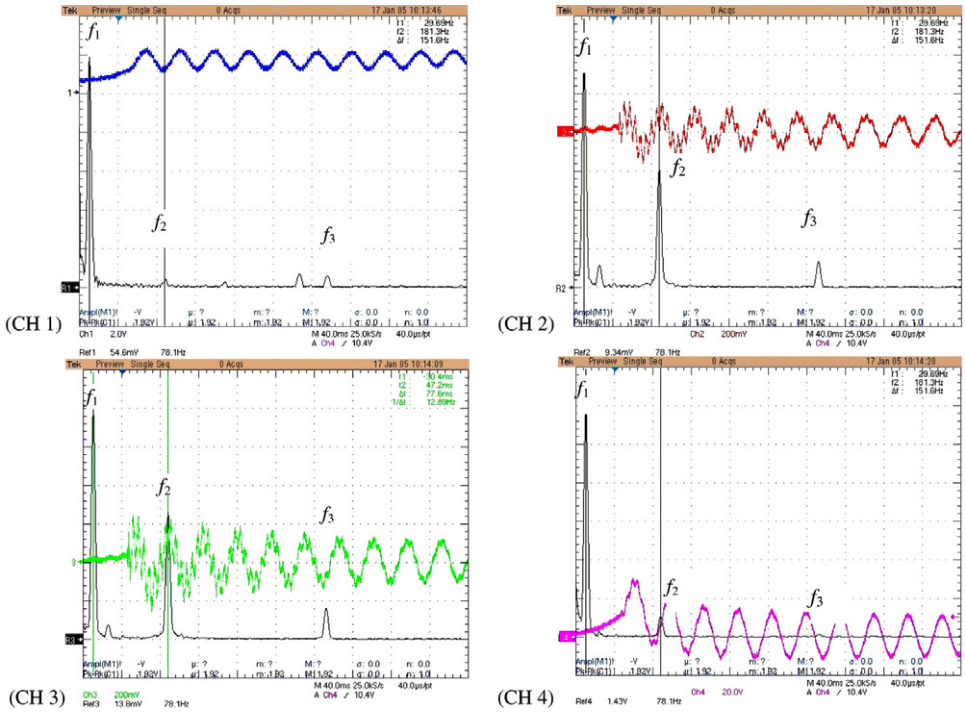

Figure 7. Vibration signal and spectrum of magnitude (Fourier transform) recorded by: (CH 1) strain gauge; (CH 2) 28 μm thick PVDF-PWAS; (CH 3) 110 μm thick PVDF-PWAS; (CH 4) 200 μm thick PZT-PWAS.

PZT-PWAS was found to give the highest voltage, but it was less responsive to the higher frequencies. The PVDF-PWAS were found to be more responsive to the high frequencies but to give a lower voltage (figure 7).

3.1.2. Data comparison and analysis. The Vishay P3 strain indicator and recorder has an analogue output from 0 to 2.5 V, which equates to strain values from -320 $\mu\varepsilon$ to $+320$ $\mu\varepsilon$. The peak-to-peak analogue output of the strain indicator was 1.32 V, which means that the peak-to-peak vibration strain equaled 338 $\mu\varepsilon$. Assuming that the oscilloscope's capacitance is 3 nF and using equation (13), the theoretical peak-to-peak voltage of PZT-PWAS, 110 μm PVDF-PWAS and 28 μm PVDF-PWAS are 30, 0.361 and 0.346 V, respectively. The experimental results can be read from table 2, which were 30.8, 0.508 and 0.332 V, respectively. The experimental response voltage (table 3) and natural frequencies (table 4) agreed with the theoretical prediction. The theoretical and experimental

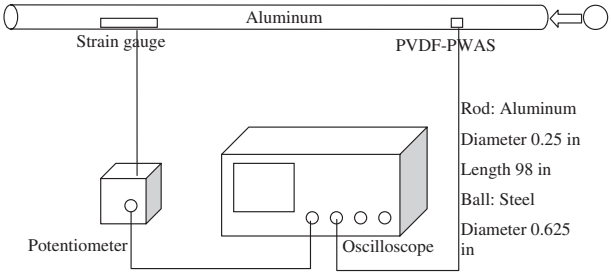

Figure 8. Experimental setup.

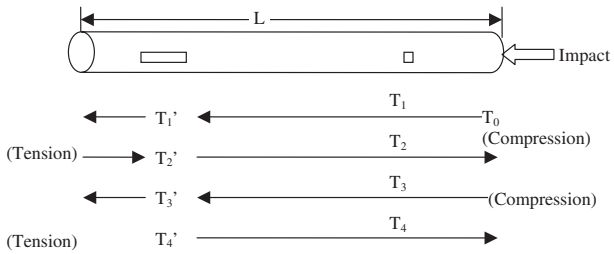

Figure 9. Stress wave propagation.

frequency values become closer with increasing frequency because of the resolution of the built-in Fourier transform of the oscilloscope.

3.2. Long rod impact test

3.2.1. Experimental setup. The PZT-PWAS, PVDF-PWAS and strain gauge for dynamic measurement were investigated on the basis of a long rod impact test. The longitudinal waves were generated by impacting the rod. The resulting waves were detected by using electrical resistance strain gauges and PVDF-PWAS.

A schematic of the apparatus is shown in figure 8. A long rod is desirable so as to lengthen the time between reflections and make the pulses more distinct. The rod was suspended in three places by a monofilament line. One strain gauge and three PVDF-PWAS were used. The Vishay BLH semiconductor-type strain gauge was mounted 23 inches (58.4 mm) from the left-hand end of the rod. This type of strain gauge was selected for its high sensitivity and good dynamic response. 7 mm square PVDF-PWAS were cut from piezo film sheets provided by Measurement Specialties, Sensor Products Division. Three PVDF-PWAS have three different thicknesses, 28, 52 and 110 μm, mounted 20 inches (50.8 mm) from the right-hand end of the rod. The impactor was a 0.625 inch (1.58 mm) diameter steel ball supported by monofilament strings. The string was adjustable so that the ball's center can be placed at the centre of the end of the rod.

There are three types of waves that can be formed upon the impact of a long rod: longitudinal waves, flexural waves, and torsional waves. If the impact is axial, the type of propagated wave is a longitudinal wave. The longitudinal wave speed propagated in a thin rod is $c = \sqrt{\frac{E}{\rho}}$, where E and ρ are the material's Young's modulus and density, respectively [27, 28]. When the impactor hits the rod at time T_0 (figure 9), the compression wave arrives at the PVDF-PWAS at time T_1, then arrives at the strain gauge at time T_1'. When the compression wave reaches the free end of the rod, it will be reflected as tension and vice versa. Stress reversal is a characteristic of the free end reflection. The tension wave will reach the strain gauge first at time T_2' and reach the PVDF-PWAS at time T_2. It will be reflected by the free end again as a compression wave.

3.2.2. Data analysis. Two pictures of the history of a strain gauge and PVDF-PWAS are shown in figures 10 and11. Figure 10 has a time base of 200 μs per division to allow recording of several transits of the wave pulse. Figure 11 is at 20 μs per division so as to observe the detail of the initial pulse more closely.

From the test, three features are apparent for the long rod. First, each cycle contains a compressive peak for the PVDF-PWAS (positive) and for the strain gauge (negative). Second, each cycle contains a tensile peak from the reflected wave for the PVDF-PWAS (negative) and the strain gauge (positive).

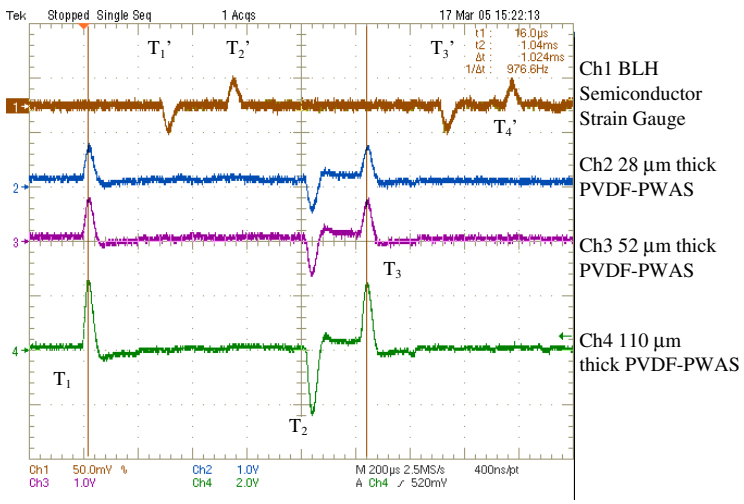

Figure 10. Impact responses for free–free boundary condition recorded by: (CH 1) strain gauge; (CH 2) 28 μm thick PVDF-PWAS; (CH 3) 52 μm thick PVDF-PWAS; (CH 4) 110 μm thick PVDF-PWAS.

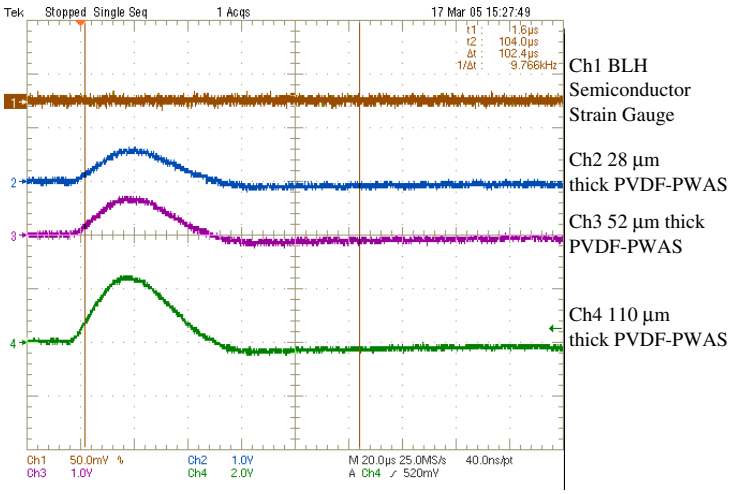

Figure 11. Impact responses recorded by: (CH 1) strain gauge; (CH 2) 28 μm thick PVDF-PWAS; (CH 3) 52 μm thick PVDF-PWAS; (CH 4) 110 μm thick PVDF-PWAS.

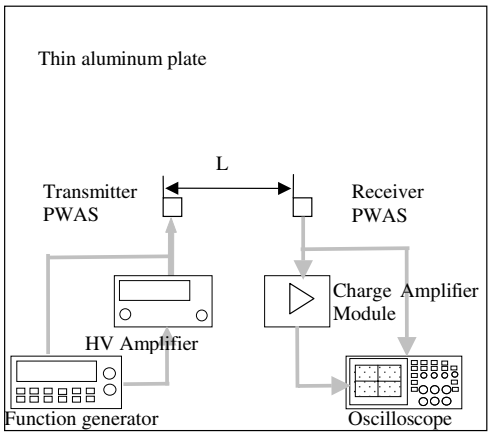

Figure 12. Two PWAS mounted on an aluminium plate: the left-hand PWAS as a transmitter; the right-hand PWAS as a receiver.

Third, there is a dwell while the wave traverses the length of the rod.

The rod is made of 6061-T6 aluminium alloy, whose Young's modulus is 69 Gpa and whose density is 2700 kg m^{-3}. The rod is 98 inches (2489 mm) in length and 0.25 inch (6.35 mm) in diameter. The theoretical velocity is $c = 5055$ m s^{-1}. The speed of the pulse moving up and down the rod can be estimated from the time between peaks. The distances traveled by the two adjacent positive or negative pulses are $2L$, where L is the length of the rod. The experimental wave speed is 4860 m s^{-1}. The relative error is 3.8%.

3.3. Pitch-catch PZT-PWAS and PVDF-PWAS experiments

3.3.1. Experimental setup. Two square (dimension: 7 mm × 7 mm × 0.2 mm) PWAS were attached to a 1200 mm × 1100 mm × 1.6 mm thin aluminium plate at a distance of L (figure 12). The left-hand PWAS was a transmitter with a smoothed 300 kHz tone-burst excitation with a 10 Hz repetition rate to generate the Lamb wave in the thin plate. It can be directly connected to an HP33120A function generator that can provide 20 V peak-to-peak excitation, or connected to a high-voltage amplifier that can provide 300 V peak-to-peak excitation. The right PWAS was a receiver to collect the Lamb wave signal. It can be connected directly to a Tektronix digital oscilloscope or connected to a charge amplifier module first then the oscilloscope. Using equation (5) and data from table 1, transmitter PZT-PWAS can generate a Lamb wave of 2 $\mu\varepsilon$ strain under 20 V peak-to-peak excitation. After the Lamb wave propagates to the receiver PZT-PWAS, the receiver PWAS can generate a 50 mV signal that can be calculated from equation (13).

Table 1. Parameters comparison table [24].

Property	Units	PZT	$BaTiO_3$	PVDF
Density	10^3 kg m^{-3}	7.5	5.7	1.78
Relative permittivity	e/e_0	1200	1700	12
d_{31} constant	(10^{-12}) C N^{-1}	110	78	23
g_{31} constant	(10^{-3}) V m N^{-1}	10	5	216
k_{31} constant	% at 1 kHz	30	21	12
Acoustic impedance	(10^6) kg m^{-2} s^{-1}	30	30	27

A complete comparison of PZT-PWAS and PVDF-PWAS in pitch-catch is shown in table 5. PZT-PWAS and PVDF-PWAS were placed at a distance of 65 mm. 'High Voltage' was selected to use to amplify the signals.

3.3.2. Charge amplifier module. A Burr-Brown precision high-speed Difet® operational amplifier OPA627 was selected for its advantage of very low noise and fast settling time. The bandwidth of the operational amplifier is 800 kHz. The PWAS capacitances were measured before and after they were attached to the plate. The free square PWAS capacitances were 3.8 nF. After PWAS were bonded to the plate, the capacitances were a little small. The measurement results were 3.25 nF for both PWAS.

Figure 13 shows the signal with and without the charge amplifier. Channel 1 was an 18 V peak-to-peak 300 kHz tone-

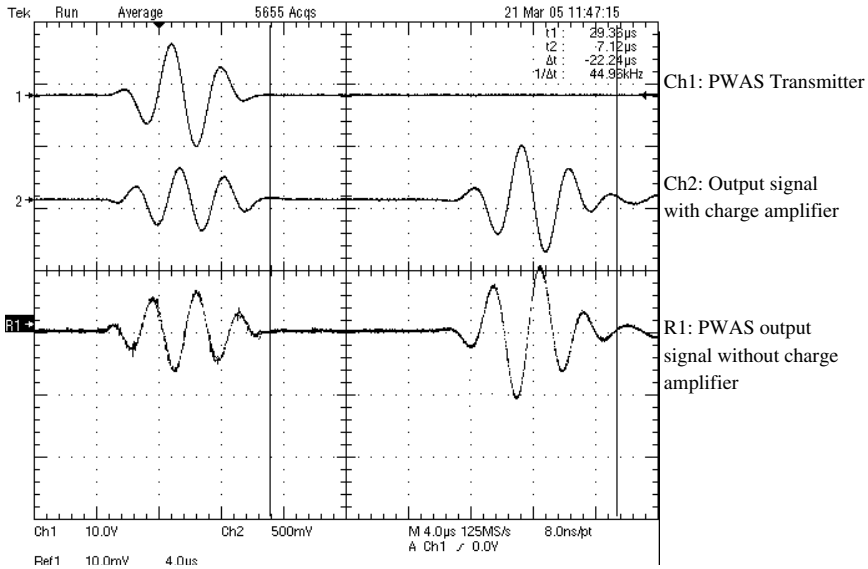

Figure 13. Charge amplifier experimental results.

Table 2. Comparison of the different sensors' responses.

Channel	Sensor	V_{pp} (V)	f_1 (Hz)	A_1 (mV)	f_2 (Hz)	A_2 (mV)	A_2/A_1 (%)	f_3 (Hz)	A_3 (mV)	A_3/A_1 (%)
CH 1	Strain gauge	1.32	29.69	327.4	182.8	12	3.66	509.4	20	6.1
CH 2	28 μm PVDF-PWAS	0.332	29.69	55.64	181.3	28.75	51.67	501.6	6.16	11.07
CH 3	110 μm PVDF-PWAS	0.508	29.69	82.5	181.3	45.65	55.33	501.6	11	13.33
CH 4	200 μm PZT-PWAS	30.8	29.69	8568	181.3	800	9.337	502.5	100	0.44

Table 3. Comparison of PWAS response.

	PZT-PWAS (V)	110 mm PVDF-PWAS (V)	28 mm PVDF-PWAS (V)
Theoretical	30	0.361	0.346
Experimental	30.8	0.508	0.332
Relative error (%)	2.67	40.7	−4.04

Table 4. Comparison of the cantilever beam natural frequency.

	f_1 (Hz)	f_2 (Hz)	f_3 (Hz)
Theoretical	28.6	179	501.3
Experimental	29.69	181.7	503.8
Relative error (%)	3.81	1.51	0.50

Table 5. Comparison of PZT-PWAS and PVDF-PWAS in pitch-catch method.

	Transmitter	HV amplifier	Input voltage (V)	Receiver	Output voltage (mV)
1	PZT	N	17	PZT	116
2	PZT	Y	57	PZT	318
3	PZT	N	17	PVDF	9.3
4	PZT	Y	57	PVDF	30.0
5	PVDF	N	18	PZT	0.96
6	PVDF	Y	57	PZT	2.1
7	PVDF	N	18	PVDF	N/A
8	PVDF	Y	250	PVDF	0.85

burst excitation signal. The Lamb wave was generated and propagated in the plate. Without the charge amplifier, the right-hand PWAS received the Lamb wave S_0 mode signal with an amplitude of 20 mV (R1). With the charge amplifier, the charge amplifier output signal was around 800 mV.

The signals in different frequency ranges were measured to determine the efficiency of the charge amplifier. In the low-frequency range from 15 to 150 kHz, the Lamb wave A_0 mode was measured because the A_0 mode was the dominant signal in this range. In the high-frequency range from 150 to 800 kHz, the Lamb wave S_0 mode was measured because S_0 was the dominant signal in this range. The voltage gain was calculated and compared with the theoretical value, as shown in figure 14.

4. Conclusion

Models of PWAS voltage-stress and voltage-strain have been introduced in this paper. The PWAS actuator-generated strain is proportional to the input voltage. The PWAS sensor response is also proportional to the derivative of the strain and stress.

Flexible PVDF-PWAS have been studied by two comparison experiments: cantilever beam free vibration and long rod impaction tests. The experimental results of the PVDF-PWAS and strain gauge have been compared with those of PZT-PWAS. The theoretical and experimental results of PZT-PWAS and PVDF-PWAS performance in this study gave a demonstration of the piezoelectricity of PWAS. The velocity of the wave propagation in an aluminium rod was obtained by applying a strain gauge and PVDF-PWAS on the surface of the rod.

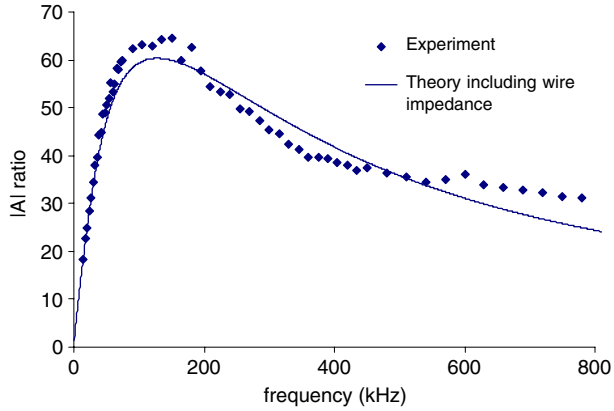

Figure 14. Comparison of the theoretical and experimental voltage gain.

Both PZT-PWAS and PVDF-PWAS are capable of use as a transmitter and receiver in the pitch-catch method. PZT-PWAS gave a higher-voltage response than PVDF-PWAS at the same condition. PVDF-PWAS was conformable to curved surfaces and more responsive to higher frequencies.

PWAS are charge mode active sensors, and we can use a charge amplifier to amplify the signal. The use of a charge-sensitive amplifier can reduce the adverse effects of low-frequency noise. From a comparison of the theoretical and experimental results, we can find that the charge amplifier was suitable for the PZT-PWAS working frequency range. The voltage gain was adjustable and the amplification ratio decreased when the frequency became high due to the connection wire impedance.

PZT-PWAS has a high capacitance of around 3 nF. PVDF-PWAS has a much lower capacitance of around 50 pF. PVDF-PWAS also give a much lower response than PZT-PWAS. A charge amplifier suitable for the PVDF-PWAS is needed.

Acknowledgments

The financial support of US National Science Foundation award no. CMS 0408578 (Dr Shih Chi Liu, program director) and US Air Force Office of Scientific Research grant no FA9550-04-0085 (Capt. Clark Allred, PhD, program manager) are gratefully acknowledged.

References

[1] Chang F-K 1995 Built-in damage diagnostics for composite structures *ICCM-10: Proc. 10th Int. Conf. on Composite Structures (Whistler, BC, Canada, Aug. 1995)* vol 5 pp 283–9

[2] Chang F-K 1998 Manufacturing and design of built-in diagnostics for composite structures *52nd Mtg Soc. Machinery Failure Prevention Technology (Virginia Beach, VA, March 1998)*

[3] Wang C S and Chang F-K 2000 Built-in diagnostics for impact damage identification of composite structures *Structural Health Monitoring 2000* ed F-K Chang (Lancaster, PA: Technomic) pp 612–21

[4] Lin X and Yuan F G 2001 Diagnostic lamb waves in an integrated piezoelectric sensor/actuator plate: analytical and experimental studies *Smart Mater. Struct.* **10** 907–13

[5] Lin X and Yuan F G 2001 Damage detection of a plate using migration technique *J. Intell. Mater. Syst. Struct.* **12** 469–82

[6] Ihn J-B and Chang F-K 2002 Built-in diagnostics for monitoring crack growth in aircraft structures *Proc. SPIE's 9th Int. Symp. Smart Structures and Materials (San Diego, CA, March 2002)* paper #4702-04

[7] Giurgiutiu V and Zagrai A 2000 Characterization of piezoelectric wafer active sensors *J. Intell. Mater. Syst. Struct.* **11** 959–76

[8] Giurgiutiu V, Zagrai A N, Bao J, Redmond J, Roach D and Rackow K 2002 Active sensors for health monitoring of aging aerospace structures *Int. J. Condition Monitoring Diagnostic Eng. Management* **5** (3)

[9] Giurgiutiu V, Bao J and Zhao W 2003 Piezoelectric-wafer active-sensor embedded ultrasonics in beams and plates *Exp. Mech.* **43** (December) 428–49

[10] Pomirleanu R and Giurgiutiu V 2004 Full-power dynamic characterization of piezoelectric and magnetostrictive actuators *J. Intell. Mater. Syst. Struct.* **15** 161–80

[11] Giurgiutiu V, Zagrai A and Bao J 2004 Damage identification in aging aircraft structures with piezoelectric wafer active sensors *J. Intell. Mater. Syst. Struct.* **15** 673–87

[12] Zhang Y 2003 Dynamic strain measurement using piezoelectric paint *4th Int. Workshop on Structural Health Monitoring (Stanford University, CA, Sept. 2003)* pp 1446–52

[13] White S R 1999 Magnetostrictive tagging of composites for health monitoring *Proc., 1999 Int. Composites Expo (Cincinnati, OH, May 1999)* pp 22E1–6

[14] Trovillion J, Kamphaus J, Quattrone R and Berman J 1999 Structural integrity monitoring using smart magnetostrictive composites *Proc., Int. Composites EXPO'99 (Cincinnati, OH, 1999)* pp 1–6 , session 22-D

[15] Egusa S and Iwasawa 1993 Piezoelectric paints: preparation and application as built-in vibration sensors of structural materials *J. Mater. Sci.* **28** 1667–72

[16] Egusa S and Iwasawa N 1998 Piezoelectric paints as one approach to smart structural materials with health-monitoring capabilities *Smart Mater. Struct.* **7** 438–45

[17] Nan C W 1994 Magnetoelectric effect in composites of piezoelectric and piezomagnetic phases *Phys. Rev.* B **50** 6072–88

[18] Pan E 2001 Exact solution for simply supported and multilayered magneto-electro-elastic plates *J. Appl. Mech.* **68** 608–18

[19] Echigoya J, Hayashi S and Obi Y 2000 Directional solidification and interface structure of $BaTiO_3$-$CoFe_2O_4$ eutectic *J. Mater. Sci.* **35** 5587–91

[20] Zheng H *et al* 2004 Multiferroic $BaTiO_3$-$CoFe_2O_4$ nanostructures *Science* **303** 661–3

[21] Cai N, Nan C-W, Zhai J and Lin Y 2004 Large high-frequency magnetoelectric response in laminated composites of piezoelectric ceramics, rare-earth iron alloys and polymer *Appl. Phys. Lett.* **84** 3516

[22] Giurgiutiu V 2004 *Micromechatronics Modeling, Analysis, and Design with Matlab* (Boca Raton, FL: CRC Press)

[23] Giurgiutiu V, Jichi F, Berman J and Kamphaus J 2001 Theoretical and experimental investigation of magnetostrictive composite beams *Smart Mater. Struct.* **10** 934–45

[24] Measurement specialties 1998 *Piezo Film Sensors Technical Manual*

[25] Whitney S 1999 *Vibrations of Cantilever Beams: Deflection, Frequency, and Research Uses*

[26] Voltera E and Zachmanoglou E C 1965 *Dynamics of Vibrations* (Columbus: Charles E Merrill Books)

[27] Graff K F 1991 *Wave Motion in Elastic Solids* (New York: Dover)

[28] Doyle J F 1998 Impact and longitudinal wave propagation *Exp. Tech.*

[29] Hamamatsu Photonics kk, solid state division *Characteristics and use of charge amplifier*